Using Mobile LiDAR Data for Rapidly Updating Road Markings

Haiyan Guan, Jonathan Li, *Senior Member, IEEE*, Yongtao Yu, Zheng Ji, and Cheng Wang, *Member, IEEE*

***Abstract*—Updating road markings is one of the routine tasks of transportation agencies. Compared with traditional road inventory mapping techniques, vehicle-borne mobile light detection and ranging (LiDAR) systems can undertake the job safely and efficiently. However, current hurdles include software and computing challenges when handling huge volumes of highly dense and irregularly distributed 3-D mobile LiDAR point clouds. This paper presents the development and implementation aspects of an automated object extraction strategy for rapid and accurate road marking inventory. The proposed road marking extraction method is based on 2-D georeferenced feature (GRF) images, which are interpolated from 3-D road surface points through a modified inverse distance weighted (IDW) interpolation. Weighted neighboring difference histogram (WNDH)-based dynamic thresholding and multiscale tensor voting (MSTV) are proposed to segment and extract road markings from the noisy corrupted GRF images. The results obtained using 3-D point clouds acquired by a RIEGL VMX-450 mobile LiDAR system in a subtropical urban environment are encouraging.**

***Index Terms*—Mobile light detection and ranging (LiDAR), point cloud, road marking, tensor voting, thresholding.**

I. Introduction

MAPPING road markings is greatly important for managing and controlling traffic activities, detecting potential road safety hazards, and improving transportation standards. According to the Manual on Uniform Traffic Control Devices (MUTCD) [1], urban roads are designed with curbstones to separate roads from sidewalks or medians. Road markings are highly reflective painted objects on the road surface. They function to guide traffic routes, control driving behaviors, and maintain traffic safeties. Rapid and accurate inventory mapping of road markings is essential to the applications of intelligent transportation systems (ITS), such as (1) Lane Departure Warning (LDW) systems, (2) anti-sleep systems, (3) driver assistance and safety warning systems [2], and (4) autonomous driving [3].

In the early stages, inventory mapping of urban road surfaces was manually accomplished by field specialists at transportation agencies. This task was labor intensive, time consuming, and costly. Remotely sensed data, such as high-resolution aerial images and recent unmanned aerial vehicle (UAV) data, have been explored for detecting roads/highways, road boundaries, and other road features and objects [4]–[6]. Frew *et al.* [6] detected lane markings from UAV images for real-time road detection using Bayesian classifier. These aerial images are still inadequate for road/highway marking inventory unless the UAV flies low enough so that road markings are clearly visible.

In recent years, mobile mapping systems using CCD cameras [7] or video cameras [8] have been developed for roadway inventory mapping. Shape, size, and color features of road markings have been used as essential cues for road marking extraction [9]–[12]. By integrating position, orientation, and intensity features, a Three-Feature based Automatic Lane Detection Algorithm (TFALDA) was proposed in [13] for detecting lane markings. This algorithm required no prior knowledge and could operate efficiently in cluttered road environments. Subsequently, multi-level feature-based approach [14] and Delaunay triangulation [15] were developed for reliably extracting lane markings. Instead of using RGB color representation, an HSI color model was proposed in [16] for lane marking detection. A method for detecting 3D zebra-crossing and dashed-line strips from stereo-pairs was presented in [17]. Image-based road marking detection methods are heavily affected by illumination changes and shadows. To obtain reliable measurements, steerable filters [18] were developed to detect road markings under varying road conditions. Real-time detection and recognition of road markings is an important issue and is urgently demanded by many activities and systems, such as Driving Assistance Systems designed to improve traffic safety. Vision-based [7], [19], curve-based [20], and feature-driven approaches [21] have been developed for real-time detection of road markings. However, these techniques highly depend on illumination conditions of the surveyed scenes and are heavily affected by noise such as pavement cracks and shadows cast by passing vehicles, roadside buildings, and trees. Therefore, image- and video-based inventory mapping techniques still face great challenges and require great improvements in order to meet the increasing demands for inspection and inventory of highways and public roads.

Manuscript received June 23, 2014; revised December 24, 2014; accepted February 27, 2015. Date of publication March 30, 2015; date of current version September 25, 2015. This work was supported in part by the Startup Foundation for Introducing Talent of Nanjing University of Information Science and Technology and the National Natural Science Foundation of China under Grants 41471379 and 41301518. The Associate Editor for this paper was Prof. U. Nunes (*Corresponding author: Jonathan Li.*)

H. Guan is with the College of Geography and Remote Sensing, Nanjing University of Information Science and Technology, Nanjing 210044, China.

J. Li is with the Fujian Key Laboratory of Sensing and Computing for Smart Cities, Xiamen University, Xiamen 361005, China, and also with the Department of Geography and Environmental Management, University of Waterloo, Waterloo, ON N2L 3G1, Canada (e-mail: junli@xmu.edu.cn; junli@uwaterloo.ca).

Y. Yu and C. Wang are with the Fujian Key Laboratory of Sensing and Computing for Smart Cities, Xiamen University, Xiamen 361005, China.

Z. Ji is with the School of Remote Sensing and Information Engineering, Wuhan University, Wuhan 430079, China.

Color versions of one or more of the figures in this paper are available online at http://ieeexplore.ieee.org.

Digital Object Identifier 10.1109/TITS.2015.2409192

Mobile light detection and ranging (LiDAR) systems have exhibited outstanding advantages over the traditional mapping techniques. Such a system is normally composed of laser scanner(s), digital camera(s), Global Positioning System (GPS), Inertial Measurement Unit (IMU), and Distance Measurement Indicator (DMI) [22]. The system can be mounted on a moving vehicle, such as a car or a train, to collect 3D geospatial data of roadways over a large area at a normal driving speed. Advantages of using mobile LiDAR for a transportation engineering survey can be summarized as (1) Safety—point clouds are collected by a vehicle moving at highway speeds, keeping surveyors off the traveled lanes. (2) Less disruptiveness—the mobile system requires no traffic controls or lane closures. (3) High accuracy—millimeter-level accuracies are possible on hard surfaces. (4) Dense data sets - extremely dense topographic data sets, consisting of approximately 1,000 measurements per square meter, and detail transportation features within the system's field of view. The data set can produce cross sections at any interval. (5) Rapid field data collection - mobile LiDAR survey data collection is significantly faster than conventional surveying methods. (6) Auxiliary imagery - digital geo-referenced imagery is collected simultaneously with the LiDAR data. Moreover, mobile LiDAR systems can complete multiple inventory mapping tasks in a single mission in a short time period. By using near-infrared spectrum, such systems are able to work day and night without considering the environmental illumination. Compared to its airborne counterparts, mobile LiDAR systems can acquire highly denser 3D point clouds, provide more direct views of road surfaces [17], and cost less for roadway inventory mapping. Therefore, mobile LiDAR systems have become a promising and cost-effective means for inventory mapping of urban road surfaces.

However, to ensure reliable results when conducting a mobile laser scanning survey, close attention must be paid to project control and targeting, data collection planning, data processing, quality assurance and quality control (QA/QC). To extract road markings from mobile LiDAR data, the first step is to identify the points belonging to road surfaces. On road surfaces, road markings are highly retro-reflective surfaces painted on roads; as a result, the reflectance of the targets in the form of intensity can be used to identify road markings [23]. Based on intensity differences between road surfaces and road markings, road markings were extracted and used in [24] as the ground control for quality assessment (QA) or quality control (QC) of the image data. In [25], a simple threshold was applied to intensity data for extracting road markings. Solid-edge-line and broken-lane-line markings were outlined in [26] by first applying an interpolation method to mobile LiDAR points, and then segmenting the image using intensity and elevation-difference information. Finally, road markings were estimated by integrating their semantic knowledge (e.g., shape and size). However, as most of these algorithms have applied a global threshold-based segmentation algorithm to the intensity data of mobile LiDAR point clouds, much noise is introduced, making these methods less effective in road-marking extraction. The intensity data highly depend on the ranges from the scanner to objects, the incidence angles of laser pulses, and the material properties of road surfaces. Thus, the intensity data need to be normalized prior to segmentation [27], [28].

In this paper, we develop a novel strategy for automated extraction of road markings from mobile LiDAR point clouds. The developed road marking extraction method is based on 2D georeferenced feature (GRF) images, which are interpolated from 3D road surface points in data pre-processing. A dynamic thresholding using Weighted Neighboring Difference Histogram (WNDH) is used for segmenting road marking candidates from GRF images. Afterwards, road markings are extracted by applying the proposed 2D multi-scale tensor voting (MSTV) framework and clustering analysis. In summary, the contributions of this paper are as follows: (1) a WNDH method for dynamically determining optimal thresholds to identify potential road marking pixels from GRF images, and (2) a novel MSTV framework for suppressing noise and extracting road markings.

The remainder of this paper is organized as follows: Section II details the workflow for extracting road markings. Section III reports and discusses the results obtained using a set of mobile LiDAR point clouds. Finally, concluding remarks are given in Section IV.

II. Strategy

The strategy for automated extraction of road markings includes two main steps: (1) data pre-processing including road surface extraction and GRF image generation; (2) road-marking extraction including dynamic thresholding, MSTV, and clustering analysis.

A. Data Pre-Processing

The mobile LiDAR point clouds acquired by our system contain both road surfaces and roadside features. Inventory mapping of road surface only focuses on road surface point clouds. In order to reduce the amount of the data being processed and the time complexity of the proposed strategy, we need to segment road surfaces from the entire point clouds rapidly and accurately. In our previous method [27], [29], we developed a curb-based approach for segmenting road surfaces. This approach first partitions point clouds into a set of blocks along the trajectory. For each of the blocks, a profile is generated perpendicularly to the trajectory. Next, each profile is vertically divided into a grid structure and a set of principal points are selected from this profile based on a layering and gradient method. Then, curb corner points are determined by calculating the slops and elevation-differences between two successive principal points. Usually, street design and construction manuals in many countries state that curb height ranges between 10 cm and 25 cm. The use of slope and elevation-difference evaluation criterion can not only remain the curb points but also remove road objects, such as cars, vans, bicycles, and pedestrians. Finally, with the constraint of the trajectory, the curb corner points determined from all profiles are fitted to form curb-lines. With the knowledge that urban roads are designed with curbstones as the boundaries of roads, road surface point cloud can be easily segmented from the entire point cloud based on the fitted curb-lines. This road surface segmentation

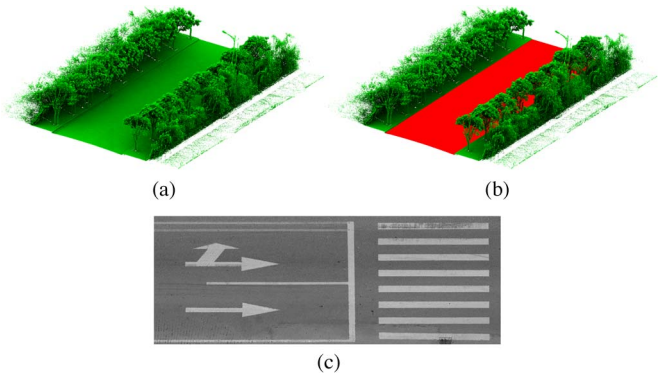

Fig. 1. (a) Raw point cloud, (b) segmented road surface (red), and (c) GRF image.

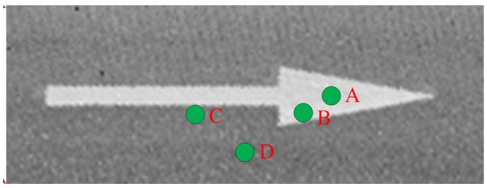

Fig. 2. Illustration of different cases for local intensity difference measure.

approach operates accurately and efficiently, therefore, in this study, we use this curb-based approach to segment road surface points. Fig. 1 shows an example of the segmented road surface.

Next, we interpolate these road surface points into a GRF image via a modified Inverse Distance Weighted (IDW) interpolation method. The modified IDW interpolation method estimates the value of a given cell by combining intensity and distance weights of all points. A detailed description and discussion of the GRF image generation and relevant parameter configurations is found in Guan *et al*. [27]. Fig. 1(c) shows an example of the generated GRF image using the IDW interpolation method.

B. Road Marking Extraction

1) WNDH-Based Dynamic Thresholding: As shown in Fig. 2, road markings show higher intensities than their surrounding road surface in the GRF image. However, the reflected laser pulse intensity highly depends on the incident angles of laser beams and the ranges between the measured target and the laser scanner. Generally, the reflected laser pulse intensity decreases with the increase of incident angles and ranges. Consequently, the road markings farther away from the scanner center exhibit relatively lower intensities than those of the road markings near to the scanner center. Therefore, the intensities of road markings distribute unevenly and show different contrasts in the GRF image.

To efficiently and completely ascertain road marking candidates, we adopt a dynamic thresholding strategy. We divide the GRF image into a set of sub-images with a size of $W_s \times W_s$ pixels. In each sub-image, we modify the Neighboring Difference Histogram (NDH) method [30] and develop a WNDH method to (1) analyze the intensity differences in a local neighborhood of each pixel, and (2) automatically determine optimal local thresholds for ascertaining road marking candidates from each of the sub-images.

Denote $I = \{S_m | m = 1, 2, ..n\}$ as the GRF image, where S_m indicates the mth sub-image and n is the number of sub-images. Denote $N(i, j)$ as the connected neighborhood with size $2k + 1 (k > 0)$ centered at pixel (i, j), and $d_m(i, j)$ as the local intensity difference measure at pixel (i, j) within sub-image $S_m (m = 1, 2, ..n)$. The local intensity difference measure is defined as follows:

$$d_m(i,j) = \frac{\sum\limits_{(u,v)\in N(i,j)} \left|I_{uv}^m - I_{ij}^m\right| \cdot \left(I_{uv}^m - I_{ij}^m\right)}{\sum\limits_{(u,v)\in N(i,j)} \left|I_{uv}^m - I_{ij}^m\right|}, \quad (1)$$

where I_{ij}^m denotes the intensity value at pixel (i, j) within sub-image S_m. The intensities along road markings are usually higher than those of the background road surface, therefore, ideally the following cases are satisfied:

(1) $d_m(i, j)$ takes a value close to zero when pixel (i, j) is located in the center area of road marking, as shown by pixel A in Fig. 2;
(2) $d_m(i, j)$ takes a negative value when pixel (i, j) is located at the internal boundary of road marking, as shown by pixel B in Fig. 2;
(3) $d_m(i, j)$ takes a positive value when pixel (i, j) is located at the external boundary of road marking, as shown by pixel C in Fig. 2;
(4) $d_m(i, j)$ takes a value close to zero when pixel (i, j) is located in the center area of the background road surface, as shown by pixel D in Fig. 2.

According to the above cases, the pixels with intensity differences in case (2) are the potential road marking candidates. To evaluate the overall intensity difference measures within each sub-image, the intensity difference measure of each pixel is aggregated to its corresponding gray level as follows:

$$H_m(l) = \sum_{I_{ij}^m = l} d_m(i,j), l \in [0, 255], \quad (2)$$

where $H_m(l)$ denotes the overall intensity difference measure of the pixels with gray level l in sub-image S_m. Then, according to the aforementioned case (2), the optimal threshold T_m for identifying road marking candidates from sub-image S_m is determined by selecting the gray level corresponding to the minimum of the overall intensity difference measure in (2), i.e.,

$$T_m = \arg\min_l H_m(l). \quad (3)$$

The pixels with intensities higher than T_m are regarded as road marking candidates.

2) MSTV-Based Road Marking Detection: Generally, the identified road marking candidates contain considerable noise. The noise is caused by the characteristics of the reflectance backscattered by the measured targets and the materials of the targets' surface. To efficiently filter out the noise, we develop

an MSTV framework which has the capability of suppressing noise and preserving road markings.

Tensor voting (TV) was first introduced in computer vision for perceptual grouping purposes [31]. A TV framework has an advanced capability to efficiently suppress high-level noise and infer perceptual structures from noisy or corrupted data. Developed on the foundation of Gestalt psychology, the TV method is based on tensor representations of image features and nonlinear voting. In the 2D case of TV, perceptual grouping is undertaken through casting votes between image primitives, such as unoriented points [32], curve elements [33], and region elements [34]. The input image primitives are first encoded as structure-aware tensors, where the structures are either regions, curves, junctions, or endpoints in the feature space [33]. Generally, a second-order, symmetric, non-negative definite tensor is represented by a 2×2 matrix, decomposed as

$$T = (\lambda_1 - \lambda_2) e_1 e_1^T + \lambda_2 \left(e_1 e_1^T + e_2 e_2^T \right) \tag{4}$$

where λ_1 and $\lambda_2 (\lambda_1 \geq \lambda_2)$ are the eigenvalues, e_1 and e_2 are the corresponding eigenvectors. A tensor is geometrically visualized as an ellipse shaped by the tensor's eigenvectors' directions and eigenvalues' magnitudes. The tensor's shape defines the structural type of interest, and its size represents the saliency. The first term in (4) is termed as stick tensor, indicating an elementary curve element with e_1 as its curve normal. The second term is called ball tensor, indicating a region structure without any preferred orientations [31]. For example, a road marking pixel in the GRF image is within a region, indicating that the pixel has no preferred orientation with the values of λ_2 in a saliency map.

Each tensor is then propagated within the voting field in the form of vote [31]. The more votes received by a given tensor, the higher the probability of a salient feature being present at the corresponding location. Each input collects all the votes cast by the tensors in its neighborhood and integrates them into a new tensor, eventually revealing behavioral coherence among the image primitives. Through tensor decomposition and eigenvalue analysis, different perceptual structures can be efficiently estimated even with the presence of high-level noise.

To efficiently extract road marking pixels from the thresholded image, we develop an MSTV framework that utilizes ball tensors to infer region elements. In a standard ball voting, image primitives are encoded with ball tensors with unit saliencies. The voting field for ball tensors is controlled by the voting scale, σ, which determines the neighborhood where a ball tensor can cast votes [31]. A large σ, which corresponds to a large voting neighborhood, enforces a higher degree of smoothness, thus assisting in noise removal. On the other hand, a small σ, which corresponds to a small voting neighborhood, has higher susceptibility to outlier corruption, but better preservation of details. Within the voting field, the vote cast by a ball tensor is achieved by summing the votes cast by stick tensors that span 360 degrees at regular intervals [35]. The vote cast by a stick tensor is defined by a decay function [31]

$$DF(s, \kappa, \sigma) = \exp\left(-\frac{s^2 + c\kappa^2}{\sigma^2} \right), \tag{5}$$

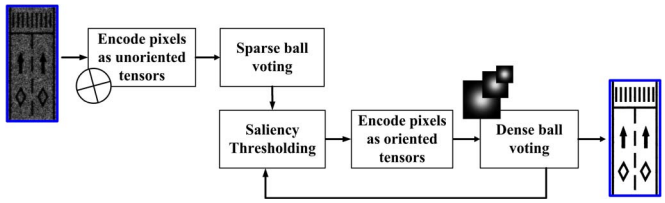

Fig. 3. Flow chart of the proposed MSTV.

where s denotes the arc length between the voter and the receiver, κ is the curvature, and c controls the degree of decay with the following form [30]

$$c = \frac{-16(\sigma - 1)\log_2 0.1}{\pi^2}. \tag{6}$$

Fig. 3 shows the flow chart of the MSTV algorithm. Assume that $P = \{p_1, p_2, p_3 \ldots, p_i, \ldots p_n\}$ is the road marking candidate data set, where n is the number of road marking candidates; p_i is the ith road marking candidate. In the MSTV framework, a road marking candidate,p_i, is initially encoded, in the form of a 2×2 identity matrix, by a ball tensor with unit saliency, since no prior distribution information is available. After construction of the tensor space, a round of sparse ball voting with σ is performed. A large σ is selected to efficiently suppress noise. An Otsu's thresholding method [36] is applied to the saliency map for removing pixels with low saliencies. After large-scale sparse ball voting, all tensors corresponding to road marking candidates obtain rough orientations and magnitudes. However, mapped road markings still contain noise and lack of saliencies. Thus, an iterative dense ball voting procedure is required to refine the results and obtain a saliency map of road markings. The first round of dense ball voting with σ is executed, followed by saliency thresholding. During the following iterations, σ is iteratively decreased by an interval $\Delta\sigma$ to focus more on preserving local details. The iterative ball voting procedure stops until the voting scale meets a stop criterion, σ_e, which allows the smallest voting field where tensors can cast votes. Therefore, with the MSTV, a refined road marking probability map is generated to enhance the road marking pixels; simultaneously, suppressing the background and the noise.

3) Road Marking Extraction: Through the MSTV framework, road markings are almost detected. However, some small fragments are falsely detected as road markings. To further remove those small noisy fragments, a region-growing approach is used to segment potential road marking pixels into separated regions. We define the criterion of the maximum distance of d_c pixels for growing two adjacent pixels. Afterwards, a bounding rectangle is calculated for each region. Then, the region whose diagonals of the bounding rectangles are smaller than a predefined threshold $d_{\min}$ are regarded as non-road markings and filtered out.

III. Results and Discussion

A. Mobile LiDAR Datasets

The data were acquired on 23 April 2012 by a RIEGL VMX-450 system. The surveyed area is in a tropical urban

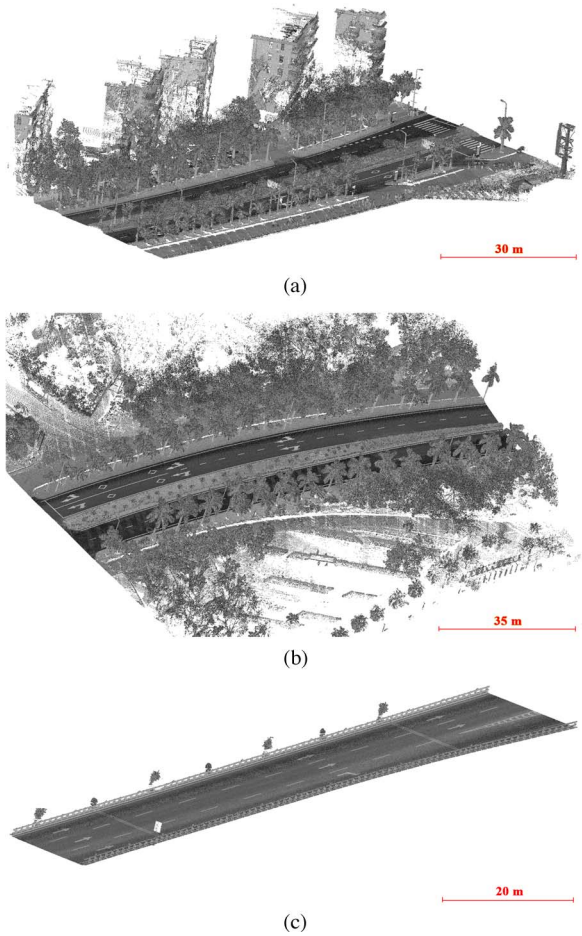

Fig. 4. Point clouds: (a) SRS dataset, (b) ICEC dataset, and (c) YB dataset.

environment, located in the City of Xiamen, southeast China. A complete survey was carried out, once in a forward direction and once in a reverse direction, on Huandao Road from Xiamen University to International Conference and Exhibition Center (ICEC), at a driving speed of approximately 50 km/h. This two-directional-four-lane Huandao road is separated by a median. This is a typical subtropical urban road area with high buildings, dense vegetation, and traffic signposts on both sides of the road. From the scanned point cloud data, three datasets were selected covering the locations of Siming Road South (SRS) [Fig. 4(a)], International Conference and Exhibition Centre (ICEC) [Fig. 4(b)], and Yanwu Bridge (YB) [Fig. 4(c)], respectively (see Table I). Using the vehicle trajectory, the road section was first segmented into road and non-road points in the pre-processing stage. Then, given that the point density on the road surface was as high as 4,000–7,000 points/m^2, 2.5-cm GSD (ground sample distance) was used for generating GRF images from the segmented road points. The GRF image sizes for the three datasets can be found in Table I.

TABLE I
DESCRIPTION OF THE THREE MOBILE LIDAR DATASETS

Dataset	Number of points	Length of road section	GRF image size (pixels)
SRS	20,180,466	142 m	3130×685
ICEC	20,701,363	155 m	3481×670
YB	7,627,886	166 m	4205×430

B. Dynamic Thresholding Tests

To evaluate the feasibility of the proposed WNDH-based dynamic thresholding, we compared it with a global thresholding method. Eight small GRF images with different types of road markings were selected in identifying road marking candidates, as shown by the first row in Fig. 5.

For our thresholding method, the window size W_s was set to be 20 pixels. First, the GRF images were virtually partitioned into a set of sub-images with the defined window width. Then, these sub-images were thresholded separately using the proposed WNDH method. The identified road marking candidates are shown in the second row in Fig. 5. For the global thresholding, a globally optimal threshold that maximizes the ratio of between-class variance to within-class variance was determined for each selected small GRF image. The identified road marking candidates are shown in the third row in Fig. 5.

The identified road marking results using the global thresholding method show that some of the road markings are missing or incomplete on one side of the GRF image, while a great portion of noise exhibits on one side of the GRF image. On the contrary, our method, which dynamically selects locally optimal thresholds, detects complete and correct road marking candidates with little noise. Visual inspection indicates that the proposed dynamic thresholding identifies road marking candidates more accurately with less noise than the global thresholding method.

To explore the impact of window size on road marking extraction, we search a range of Ws (5, 10, 20, 30, 40, 50, 60, 70, 80 pixels) for the eight GRF images. By comparing the extracted road markings with the manually interpreted ground-truth, we quantitatively evaluated the results of the extracted road markings using the following three measures: completeness, correctness, and F-measure [22].

Fig. 6 shows the measures of road marking extraction results on the eight images with nine different window sizes. The results of all eight samples demonstrate that the *completeness* index increases when the window size increases from 5 to 30, while the *completeness* decreases slightly when the window size is over 40. The *correctness* index, on the contrary, decreases with the increase of the window size. Accordingly, F-measure remains relatively stable. Over the window size of 50, the correctness tends to increase, while F-measure decreases. In our study, with an image resolution of 2.5 cm, the best window size was obtained at $W_s = 40 - 50$.

C. Synthetic Data Tests on MSTV

To test the capability of the proposed MSTV framework in suppressing noise and preserving perceptual structures, a set of synthetic images, which contain different levels of signal to noise ratios (SNR), were used for road marking extraction. Generally, the smaller the SNR, the higher the noise level. A range of SNR (e.g. 0.1, 0.2, 0.5, 1.0, 2.0, 5.0, 10.0) was applied to the original synthetic image without noise. In the

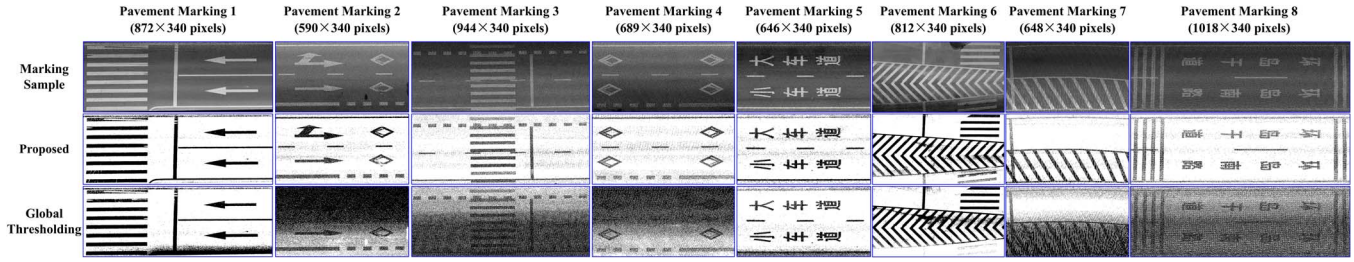

Fig. 5. Identified road marking candidates with different thresholding methods.

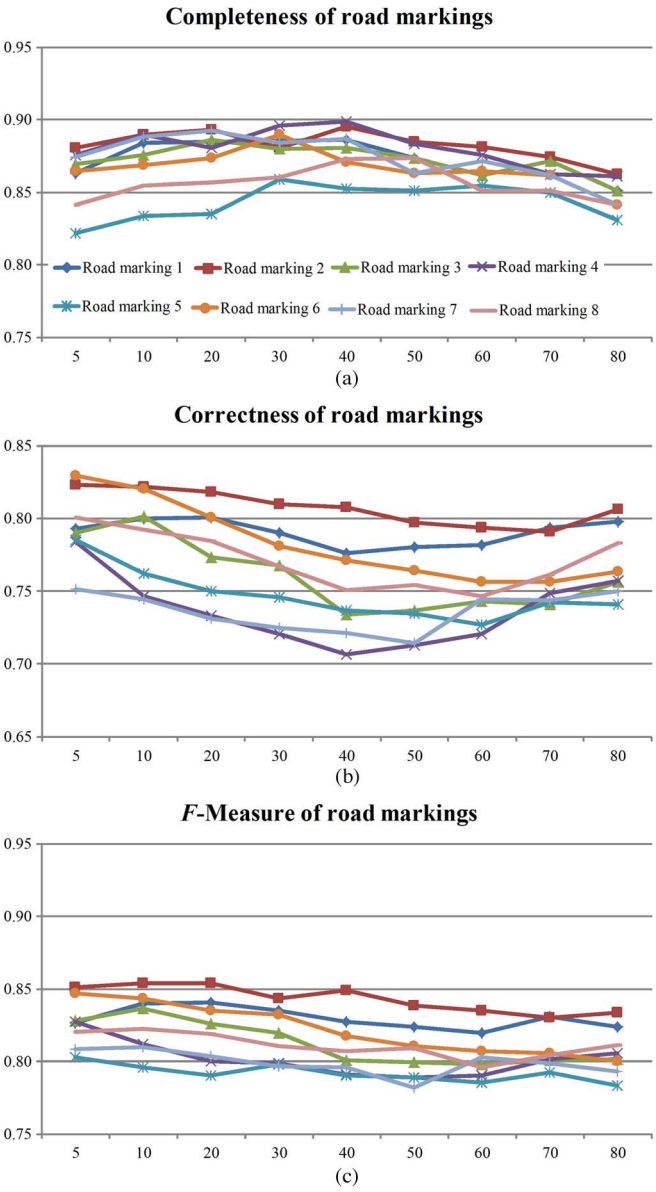

Fig. 6. Eight GRF images with different window sizes, ranging from 5 to 80 pixels, (a) completeness, (b) correctness, and (c) F-measure.

MSTV, the following parameters are used: σ, $\Delta\sigma$, and σ_e. Among these three parameters, the scale of voting, σ, controls the neighborhood sizes for both the sparse ball voting and the first dense ball voting in the iterations. σ_e and $\Delta\sigma$ are used to control the number of iterations.

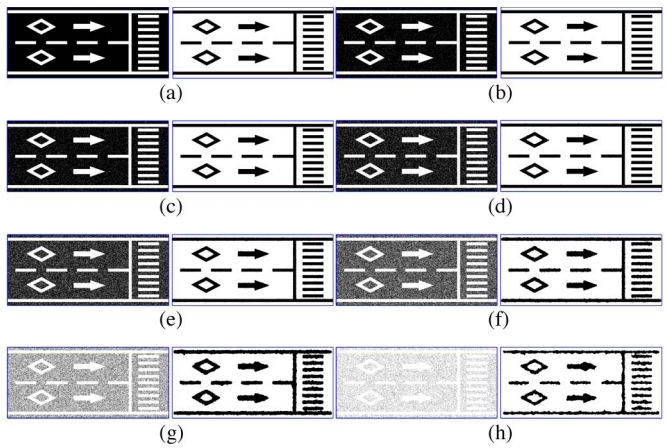

Fig. 7. Illustration of testing MSTV: (a) synthetic images without noise, (b) SNR = 10.0, (c) SNR = 5.0, (d) SNR = 2.0, (e) SNR = 1.0, (f) SNR = 0.5, (g) SNR = 0.2, and (h) SNR = 0.1.

In Fig. 7, the left images indicate the synthetic images corrupted with noises with different variances. The processing parameters are $\sigma = 14$, $\Delta\sigma = 4.5$, and $\sigma_e = 5$. The right images present the extracted road markings by using the proposed MSTV framework. As shown in Fig. 7, when the SNR is relatively high (SNR ≥ 0.5), noise is well suppressed, thereby resulting in good extraction results. The capability of our method decreases with the decrease of the SNR (SNR $= 0.2$ and SNR $= 0.1$). However, the extraction results are still acceptable with the existence of such high-level noise. Therefore, the proposed MSTV framework is robust to suppress noise, and obtains acceptable extraction results even with low SNRs.

D. Overall Performance

To examine the performance of the proposed method, the selected datasets (SRS, ICEC, and YB datasets in Section III-A were used to extract road markings. The GRF images for the three datasets are shown in Figs. 8(a), 9(a), and 10(a), respectively. The parameters and their configurations used in road marking extraction are listed in Table II.

With the optimal window size of 50 pixels aforementioned in Section III-B, the proposed WNDH-based dynamic thresholding method was used to identify road marking candidates from GRF images, as shown in Figs. 8(b), 9(b), and 10(b), respectively. By using dynamic thresholding, road marking candidates were identified with little incompleteness and noise.

Afterwards, the identified road marking candidates were processed through the MSTV algorithm to iteratively suppress

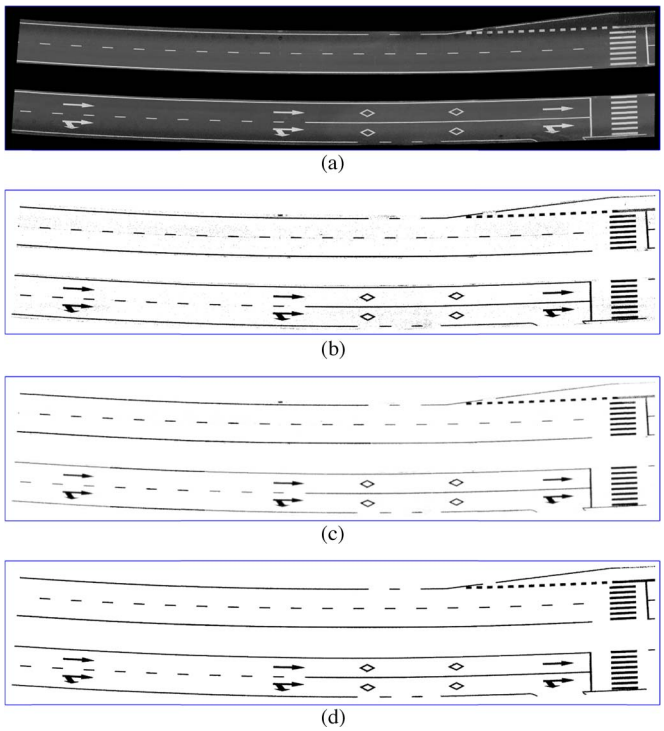

Fig. 8. (a) A GRF image, (b) identified road marking candidates, (c) saliency map, and (d) extracted road markings.

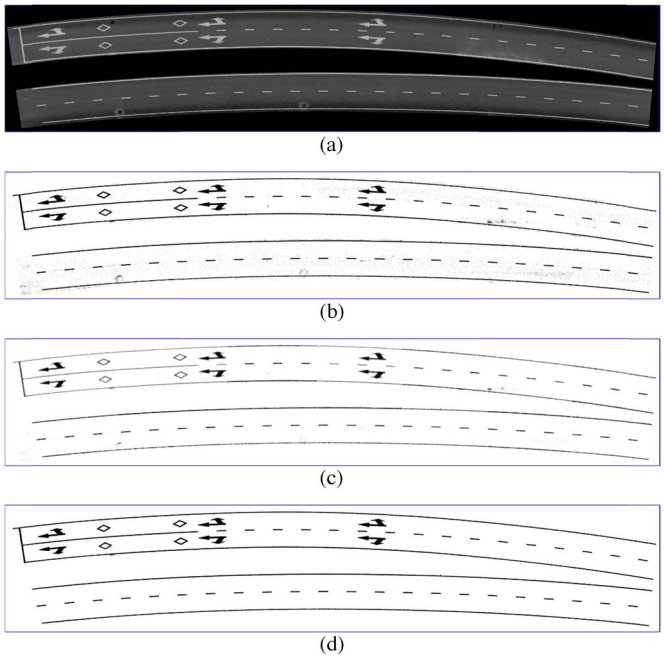

Fig. 9. (a) A GRF image, (b) identified road marking candidates, (c) saliency map, and (d) extracted road markings.

noise. A saliency map was generated for each dataset using the saliencies of ball tensors, as shown in Figs. 8(c), 9(c), and 10(c), respectively. In the saliency maps, the darker the pixel, the higher the probability of that pixel being located within the region of road markings, while the brighter the pixel, the higher the probability of that pixel being noise. As seen from the saliency maps, noise is well suppressed and road markings are well preserved and enhanced. Finally, road markings were accurately extracted after removing small fragments that are unlikely to be road markings. The extracted road markings are shown in Figs. 8(d), 9(d), and 10(d), respectively. As seen from the extraction results, road markings are accurately extracted with little loss and incompleteness.

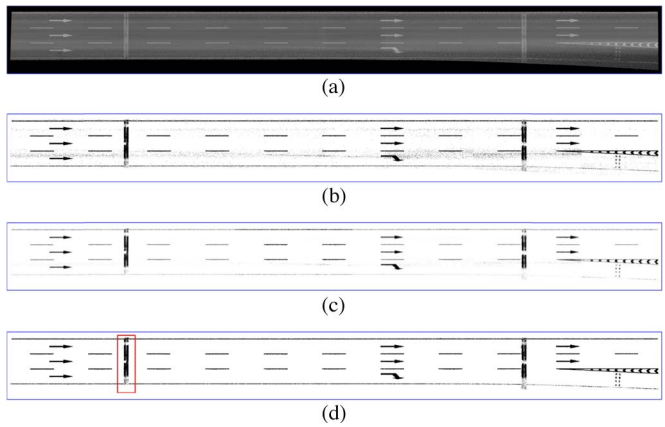

Fig. 10. (a) A GRF image, (b) identified road marking candidates, (c) saliency map, and (d) extracted road markings.

TABLE II
PARAMETER CONFIGURATIONS IN ROAD MARKING EXTRACTION

Notation	W_S	κ	σ	$\Delta\sigma$	σ_e	d_c	$d_{\min}$
Value	40 pixels	1 pixel	14.0	4.5	5.0	2 pixels	20 pixels

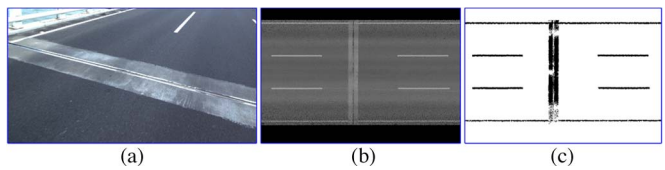

Fig. 11. Illustration of commission error in YB dataset: (a) Scene image, (b) a GRF image, and (c) extracted road markings.

TABLE III
QUANTITATIVE EVALUATION RESULTS FOR ROAD MARKING DATASETS

Evaluation \ Dataset	SRS	ICEC	YB	Average
Completeness	0.96	0.96	0.87	0.93
Correctness	0.93	0.93	0.78	0.88
F-measure	0.95	0.94	0.82	0.90

Observed from the extracted results, different types of road markings are correctly extracted. However, as shown by the red rectangle in Fig. 10(d), some of the pixels were falsely detected as road markings. Since the special material of the bridge joint [Fig. 11(a)], the pixels belonging to this region show high intensities in the GRF image [Fig. 11(b)]. Thus, these pixels are falsely detected as road markings [Fig. 11(c)].

Next, to quantitatively evaluate the performance of the proposed road marking extraction method, three measures were used: completeness, correctness, and F-measure. The quantitative evaluation results are detailed in Table III. For the three

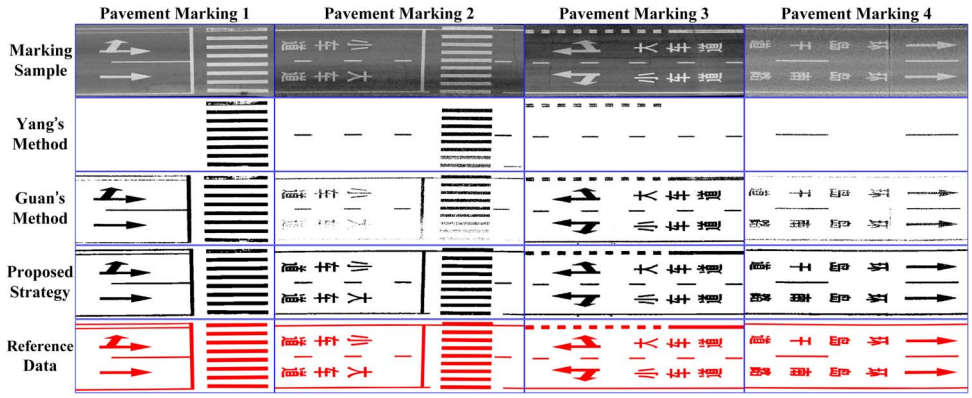

Fig. 12. Extracted pavement markings using different methods.

datasets, the proposed strategy achieves an average completeness of 0.93, an average correctness of 0.88, and an average F-measure of 0.90. The proposed strategy shows high performance on SRS and ICEC datasets, while a relatively lower performance occurs on YB dataset caused by the commission errors on the bridge joints. On the whole, our method performs very well and extracts road markings accurately and completely.

E. Comparative Study

A comparative study was carried out to compare our pavement marking extraction strategy with two recently published methods, i.e., Yang's method [26] and Guan's method [27]. The pavement marking datasets selected for this comparative study are shown in the first row in Fig. 12. The pavement marking extraction results using Yang's method, Guan's method, and our proposed strategy are shown in the second, third, and fourth rows, respectively. Comparing the extraction results using different methods with the manually labeled reference data (see the last row in Fig. 12), we conclude that Yang's method can only extract isolated small-size rectangular-shaped pavement markings, while Guan's method and our proposed strategy can extract different types of pavement markings. Furthermore, compared to Guan's method, our proposed strategy can extract pavement markings more completely and accurately with less commission and omission errors. Affected by using MSTV, our proposed strategy takes longer computing time than Guan's method in extracting pavement markings. However, benefited from the characteristics of TV, the voting process of each tensor can be carried out separately and independently. Therefore, multi-thread and parallel computing techniques can be used to further reduce the time complexity and improve the performance of our strategy for road marking extraction.

F. Time Complexity Analysis

The proposed strategy for inventory mapping of urban road surfaces was implemented using $C++$ running on an Intel (R) Core (TM) i5-3470 computer with 16.0 GB memory. The computing time in each step was recorded to analyze the time complexity of the proposed strategy. Table IV lists the computing time in each step as well as the total computing time for road marking extraction. As seen from Table IV, MSTV takes the majority of the total computing time. Therefore, the time complexity of the proposed strategy is basically determined by the MSTV. However, for the road marking datasets, the computing time is acceptable for accurately and completely extracting road markings from such big, noisy, and intensity-imbalanced GRF images. Since each road marking candidate operates separately and independently in the MSTV, multi-thread or parallel computing techniques were used to further reduce the time complexity of the proposed MSTV. We have explored the parallel method for process virtualization of large-scale laser scanning data in a cloud computing environment [33]. Six nodes were used in this study. Accordingly, we built six threads to demonstrate the effectiveness of the multi-thread strategy for easy comparison. As shown in Table IV, compared to the sequential processing strategy, the multi-thread and the parallel processing strategies dramatically reduce the computation complexity by 84% and 65%, respectively.

TABLE IV
COMPUTING TIME IN SECONDS FOR ROAD MARKING DATASETS

Datasets / Processing mode	SRS	ICEC	YB
Sequential processing time (MSTV)	205.78 (197.95)	221.50 (213.18)	127.60 (121.81)
Multi-thread processing time (6 threads)	41.95	45.73	27.62
Parallel processing time (6 nodes)	73.12	78.69	45.67

IV. CONCLUDING REMARKS

In this paper, we have proposed a novel strategy for rapid update of road markings from mobile LiDAR point clouds. Our strategy has been applied to three mobile LiDAR datasets for extracting road markings. Through visual inspection and quantitative evaluation, our strategy achieved an average completeness of 0.93, an average correctness of 0.88, and an average F-measure of 0.90. Moreover, a comparative study has been conducted to compare the performance and accuracy of our strategy with those existing methods. The comparative results demonstrate that our strategy extracts road markings more accurately and completely with less commission and omission errors. However, by using MSTV, our strategy takes longer computing time to extract road markings. By the nature of TV,

the voting process of each tensor can be carried out separately and independently. Time complexity analysis shows that the use of multi-thread and parallel computing techniques in the MSTV can dramatically reduce the processing time, thereby improving computation efficiency for inventory mapping of urban road surfaces.

ACKNOWLEDGMENT

The authors would like to acknowledge the anonymous reviewers for their valuable comments.

REFERENCES

[1] Manual on Uniform Traffic Control Devices for Streets and Highways, 2009 Edition, DOT, Washington, DC, USA, 2012, (accessed 07. 12. 2013). [Online]. Available: http://mutcd.fhwa.dot.gov/pdfs/2009r1r2/mutcd2009r1r2edition.pdf

[2] N. Zheng, S. Tang, H. Cheng, Q. Li, G. Lai, and F. Y. Wang, "Toward intelligent driver-assistance and safety warning system," *IEEE Intell. Syst.*, vol. 19, no. 2, pp. 8–11, Mar./Apr. 2004.

[3] H. Cheng, N. Zheng, X. Zhang, and J. Qin, "Interactive road situation analysis for driver assistance and safety warning systems: Framework and algorithms," *IEEE Trans. Intell. Transp. Syst.*, vol. 8, no. 1, pp. 157–167, Mar. 2007.

[4] H. Zhou, H. Kong, L. Wei, D. Creighton, and S. Nahavandi, "Efficient road detection and tracking for unmanned aerial vehicle," *IEEE Trans. Intell. Transp. Syst.*, vol. 16, no. 1, pp. 297– 309, Feb. 2015.

[5] C. Zhang, "An unmanned aerial vehicle-based imaging system for 3D measurement of unpaved road surface distresses," *Comput.-Aided Civil Infrast. Eng.*, vol. 27, no. 2, pp. 118–129, Feb. 2012.

[6] E. Frew, T. McGee, Z. Kim, X. Xiao, S. Jackson, M. Morimoto, S. Rathinam, J. Padial, and R. Sengupta. "Vision-based road following using a small automonous aircraft," in *Proc. IEEE Aerosp. Conf.*, 2004, pp. 3006– 3015.

[7] A. Broggi, "A massively parallel approach to real-time vision-based road markings detection," in *Proc. Intell. Veh. Symp.*, Detroit, MI, USA, Sep. 25–26, 1995, pp. 84–89.

[8] J. McCall and M. Trivedi, "Video-based lane estimation and tracking for driver assistance: Survey, system, and evaluation," *IEEE Trans. Intell. Transp. Syst.*, vol. 7, no. 1, pp. 20–37, Mar. 2006.

[9] Y. He, H. Wang, and B. Zhang, "Color-based road detection in urban traffic scenes," *IEEE Trans. Intell. Transp. Syst.*, vol. 5, no. 4, pp. 309–318, Dec. 2004.

[10] M. Revilloud, D. Gruyer, and E. Pollard, "An improved approach for robust road marking detection and tracking applied to multi-lane estimation," in *Proc. IEEE IV Symp.*, Gold Coast, Australia, Jun. 23–36, 2013, pp. 783–790.

[11] B. Qin, W. Liu, X. Shen, Z. Chong, T. Bandyopadhyay, M. H. Ang lr., E. Frazzoli, and D. Rus, "A general framework for road marking detection and analysis," in *Proc. 16th Int. IEEE ITSC*, Hague, Netherlands, Oct. 6–9, 2013, pp. 619–625.

[12] T. Veit, J. Tarel, P. Nicolle, and P. Charbonnier, "Evaluation of road marking feature extraction," in *Proc. 11th Int. IEEE Conf. Intell. Transp. Syst.*, Beijing, China, Oct. 12–15, 2008, pp. 174–181.

[13] Y. Yim and S. Oh, "Three-Feature Based Automatic Lane Detection Algorithm (TFALDA) for autonomous driving," *IEEE Trans. Intell. Transp. Syst.*, vol. 4, no. 4, pp. 219– 225, Dec. 2003.

[14] P. Lindner, S. Blokzyl, G. Wanielik, and U. Scheunert, "Applying multi level processing for robust geometric lane feature extraction," in *Proc. IEEE Conf. MFI*, Salt Lake City, UT, USA, Sep. 5–7, 2010, pp. 248–254.

[15] S. Abe, K. Shoji, F. Toyama, and J. Miyamichi, "Lane marking detection by extracting white regions with predefined width from bird's-eye road images," in *Proc. IS&T/SPIE Electron. Imag.*, Jan. 24, 2011, Art. ID. 78780T.

[16] T. Sun, S. Tsai, and V. Chan, "HSI color model based lane-marking detection," in *Proc. IEEE Intell. Transp. Syst. Conf.*, Toronto, ON, Canada, Sep. 17–21, 2006, pp. 1168–1172.

[17] B. Soheilian, N. Paparoditis, D. Boldo, and J. P. Rudant, "Automatic 3D extraction of rectangular roadmarks with centimeter accuracy from stereo-pairs of a ground-based mobile mapping system," in *Proc. ISPRS Arch.*, 2007, vol. 36(-5/C55), pp. 22–27.

[18] J. McCall and M. Trivedi, "An integrated, robust approach to lane marking detection and lane tracking," in *Proc. IEEE Intell. Veh. Symp.*, Parma, Italy, Jun. 14–17, 2004, pp. 533–537.

[19] W. Liu, H. Zhang, B. Duan, and H. Yuan, "Vision-based real-time lane marking detection and tracking," in *Proc. 11th Int. Conf. Intell. Transp. Syst.*, Beijing, China, Oct. 12–15, 2008, pp. 49–54.

[20] G. Maier, S. Pangerl, and A. Schindler, "Real-time detection and classification of arrow markings using curve-based prototype fitting," in *Proc. IEEE Intell. Veh. Symp.*, Baden-Baden, Germany, Jun. 5–9, 2011, pp. 442–447.

[21] A. Kheyrollahi and T. Breckon, "Automatic real-time road marking recognition using a feature driven approach," *Mach. Vis. Appl.*, vol. 23, no. 1, pp. 123–133, Jan. 2012.

[22] K. Williams, M. Olsen, G. Roe, and C. Glennie, "Synthesis of transportation applications of mobile LiDAR," *Remote Sens.*, vol. 5, no. 9, pp. 4652–4692, Sep. 2013.

[23] X. Chen, B. Kohlmeyer, M. Stroila, N. Alwar, R. Wang, and J. Bach, "Next generation map marking: Geo-referenced ground-level LiDAR point clouds for automatic retro-reflective road feature extraction," in *Proc. 17th ACM SIGSPATIAL Int. Conf. Adv. Geogr. Inf. Syst.*, Seattle, WA, USA, Nov. 4–6, 2009 , pp. 488–491.

[24] C. Toth, E. Paska, and D. Brzezinska "Using road pavement markings as good control for LiDAR data," in *Proc. ISPRS Arch.*, 2008, vol. 37(B1), pp. 189–196.

[25] L. Smadja, J. Ninot, and T. Gavrilovic, "Road extraction and environment interpretation from LiDAR sensors," in *Proc. ISPRS Arch.*, 2010, vol. 38, pp. 281–286.

[26] B. Yang, L. Fang, Q. Li, and J. Li, "Automated extraction of road markings from mobile lidar point clouds," *Photogramm. Eng. Remote Sens.*, vol. 78, no. 4, pp. 331–338, Apr. 2012.

[27] H. Guan, J. Li, Y. Yu, C. Wang, M. A. Chapman, and B. Yang, "Using mobile laser scanning data for automated extraction of road markings," *ISPRS J. Photogramm. Remote Sens.*, vol. 87, pp. 93–107, Jan. 2014.

[28] G. Vosselman, "Advanced point cloud processing," *Photogramm. Week*, Heidelberg, Germany, Sep. 7–11, 2009, pp. 137–146.

[29] Y. Yu, J. Li, H. Guan, F. Jia, and C. Wang, "Learning hierarchical features for automated extraction of road markings from 3D mobile LiDAR point clouds," *IEEE J. Sel. Topics Appl. Earth Observ. Remote Sens.*, vol. 8, no. 2, DOI: 10.1109/JSTARS.2014.2347276, Feb. 2015.

[30] Q. Li, Q. Zou, D. Zhang, and Q. Q. Mao, "FoSA: F∗ seed-growing approach for crack-line detection from pavement images," *Image Vis. Comput.*, vol. 29, no. 12, pp. 861–872, Nov. 2011.

[31] P. Mordohai and G. Medioni, *Tensor Voting: A Perceptual Organization Approach to Computer Vision and Machine Learning*. San Rafael, CA, USA: Morgan & Claypool Publ., 2006.

[32] D. Gong and G. Medioni, "Probabilistic tensor voting for robust perceptual grouping," in *Proc. IEEE CVPRW*, Providence, RI, USA, Jun. 16–21, 2012, pp. 1–8.

[33] L. Loss, G. Bebis, and B. Parvin, "Iterative tensor voting for perceptual grouping of ill-defined curvilinear structures," *IEEE Trans. Med. Imag.*, vol. 30, no. 8, pp. 1503–1513, Aug. 2011.

[34] W. Tong, C. Tang, P. Mordohai, and G. Medioni, "First order augmentation to tensor voting for boundary inference and multiscale analysis in 3D," *IEEE Trans. Pattern Anal. Mach. Intell.*, vol. 26, no. 5, pp. 594–611, May 2004.

[35] Q. Zou, Y. Cao, Q. Li, Q. Mao, and S. Wang, "CrackTree: Automatic crack detection from pavement images," *Pattern Recognit. Lett.*, vol. 33, no. 3, pp. 227–238, Feb. 2012.

[36] N. Otsu, "A threshold selection method from gray-level histograms," *IEEE Trans. Syst., Man, Cybern.*, vol. SMC-9, no. 1, pp. 62–66, Jan. 1979.

Haiyan Guan received the Ph.D. degree in photogrammetry and remote sensing from Wuhan University, Wuhan, China and the Ph.D. degree in geomatics from the University of Waterloo, Waterloo, ON, Canada in 2010 and 2014, respectively. She is currently a Professor with Nanjing University of Information Science and Technology, Nanjing, China. She is the author or coauthor of more than 30 research papers published in refereed journals, books, and proceedings. Her research interests include airborne, terrestrial, and mobile laser scanning data processing algorithms and 3-D spatial modeling and reconstruction of critical infrastructure and landscape.

Jonathan Li (M'00–SM'11) received the Ph.D. degree in remote sensing from the University of Cape Town, South Africa.

He is currently a Professor with the Department of Geography and Environmental Management, University of Waterloo, Waterloo, ON, Canada. He is also a Professor and Director of the Fujian Key Laboratory of Sensing and Computing for Smart Cities, Xiamen University, Xiamen, China. He has published extensively in leading remote sensing journals. His current research interests include mobile laser scanning point cloud processing, feature extraction and 3D surface modeling. Dr. Li is Chair of ISPRS ICWG I/Va on Mobile Scanning and Imaging Systems (2012–2016), Vice Chair of ICA Commission on Mapping from Remote Sensor Imagery (2011–2015), Vice Chair of FIG Commission IV on Hydrography and the Chair of FIG WG4.4 on Maritime and Marine Spatial Information Management (2015–2018).

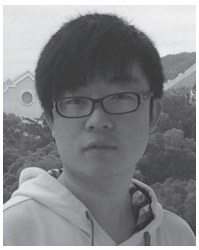

Yongtao Yu received the B.Sc. degree in computer science and technology from Xiamen University, Xiamen, China, in 2010. He is currently working toward the Ph.D. degree with the School of Information Science and Engineering, Xiamen University. His current research interests include computer vision, pattern recognition, machine learning, mobile laser scanning, and point cloud processing. He has published over a dozen of papers in refereed journals and conferences.

Zheng Ji received the Ph.D. degree in photogrammetry and remote sensing from Wuhan University, Wuhan, China, in 2007. He is currently an Associate Professor with the School of Remote Sensing and Information Engineering, Wuhan University, China and a visiting scholar with Prof. J. Li at the Department of Geography and Environmental Management, University of Waterloo, Waterloo, Ontario, Canada (2015–2016). His research interests include terrestrial lidar data processing and close-range photogrammetry, and unmanned aerial vehicle data processing. He has published over 30 papers in refereed journals and conferences.

Cheng Wang (M'12) received the Ph.D. degree in information and communication engineering from the National University of Defense Technology, Changsa, China. He is currently a Professor with the Department of Computer Science, and an Associate Dean in Research with the School of Information Science and Engineering, Xiamen University, Xiamen, China. His current research interests include remote sensing image processing, mobile mapping data analysis, multisensor fusion and information extraction from point clouds. He has published almost 100 papers in refereed journals and conferences. He is currently Co-Chair of ISPRS WG I/3 on Multi-Platform Multi-Sensor System Calibration (2012–2016). He is also the Executive Director of the Fujian Key Laboratory of Sensing and Computing for Smart Cities, Xiamen University, Xiamen, China.